Comparison of the Hazard Mapping System (HMS) Fire Product to Ground-based Fire Records in Georgia, USA

Xuefei Hu[1], Chao Yu[1,2], Di Tian[3], Mark Ruminski[4], Kevin Robertson[5], Lance A. Waller[6], Yang Liu[1]*

[1] Department of Environmental Health, Rollins School of Public Health, Emory University, Atlanta, GA 30322, USA

[2] now at Tsinghua University, Beijing, China

[3] Environmental Protection Division, Georgia Department of Natural Resources, Atlanta, Georgia

[4] NOAA/National Environmental Satellite, Data, and Information Service, College Park, Maryland 20740

[5] Tall Timbers Research Station, 13093 Henry Beadel Dr., Tallahassee, FL 32312, USA

[6] Department of Biostatistics & Bioinformatics, Rollins School of Public Health, Emory University, Atlanta, GA 30322, USA

* Corresponding Author:

Yang Liu

Department of Environmental Health

Rollins School of Public Health

Emory University

Atlanta, GA 30322, USA

Tel: 404-727-2131, Fax: 404-727-8744

E-mail: yang.liu@emory.edu

Key Points

- We compared 2011 HMS fire pixels to ground-based fire records in Georgia.
- The fire detection rate increases from 3% to 80% with the increase of fire size.
- Detection rates are higher for seasons and LULC types prone to large fires.

Comparison of the Hazard Mapping System (HMS) Fire Product to Ground-based Fire Records in Georgia, USA

Abstract: Biomass burning has a significant and adverse impact on air quality, climate change, and various ecosystems. The Hazard Mapping System (HMS) detects fires using data from multiple satellite sensors in order to maximize its fire detection rate. However, to date, the detection rate of the HMS fire product for small fires has not been well studied, especially using ground-based fire records. This paper utilizes 2011 fire information compiled from ground observations and burn authorizations in Georgia to assess the comprehensiveness of the HMS active fire product. The results show that detection rates of the hybrid HMS increase substantially by integrating multiple satellite instruments. The detection rate increases dramatically from 3% to 80% with an increase in fire size from less than 0.02 km^2 to larger than 2 km^2, resulting in detection of approximately 12% of all recorded fires which represent approximately 57% of the total area burned. The spatial pattern of detection rates reveals that grid cells with high detection rates are generally located in areas where large fires occur frequently. The seasonal analysis shows that overall detection rates in winter and spring (12% and 13%, respectively) are higher than those in summer and fall (3% and 6%, respectively), mainly because of higher percentages of large fires (> 0.19 km^2) that occurred in winter and

spring. The land cover analysis shows that detection rates are 2-7 percentage points higher in land cover types that are prone to large fires such as forestland and shrub land.

Keywords: HMS, biomass burning, ground records, and comparison

1. Introduction

Biomass burning releases large volumes of trace gases, including carbon monoxide (CO), carbon dioxide (CO_2), and methane (CH_4), and aerosols into the atmosphere, which can have a significant impact on air quality [*Sapkota et al.*, 2005] and climate change [*Fearnside*, 2000; *Lin et al.*, 2006]. In addition, wildfires have profound influence on various ecosystems and can lead to alteration of forest structure, degradation of biodiversity [*Slik et al.*, 2008] and erosion of forest soils [*Certini*, 2005]. Hence, obtaining accurate locations and sizes of various fires is crucial for assessing their contributions to air pollution, environmental degradation, and climate change.

Recording wildland fire events, whether prescribed burning or wildfires, using field measurements is time-consuming and expensive, and often not feasible across large regions. With its comprehensive spatiotemporal coverage, satellite remote sensing is capable of providing observations of active fire spots on both regional and global scales by detection of thermal infrared radiation from the Earth's surface. To date, several satellite-derived fire detection

products are available, including those from Moderate Resolution Imaging Spectroradiometer (MODIS) [*Giglio et al.*, 2003; *Justice et al.*, 2002], Geostationary Operational Environmental Satellite (GOES) [*Prins and Menzel*, 1992; 1994; *Zhang and Kondragunta*, 2008], Advanced Very High Resolution Radiometer (AVHRR) [*Stroppiana et al.*, 2000], and Visible Infrared Imaging Radiometer Suite (VIIRS) [*Csiszar et al.*, 2014]. However, active fire detections from a single satellite instrument often omit a large number of fires, especially small fires. Small fires are presumably less detectable because they are shorter in duration and may be missed by satellite flyovers, and they have lower rates of energy release per fire event. Correspondingly, previous studies reported increased fire detection rates with increased fire size. Detection rates range from very low (typically < 20%) for fires in the tens of hectares to upwards of 80% for fires covering hundreds of hectares using MODIS [*Hantson et al.*, 2013], GOES [*Schroeder et al.*, 2008a], AVHRR [*Boles and Verbyla*, 2000], and VIIRS [*Oliva and Schroeder*, 2015]. Given the different nominal sensor resolution between the geostationary and polar sensors used in this study (4 km GOES imager vs 1 km AVHRR and MODIS, respectively), it is not surprising that smaller fires would be more readily detected by the polar instruments. However, the more rapid GOES refresh allows greater opportunity for GOES to detect fires that burn for a shorter period of time. Integrating active fire spots derived from multiple satellite sensors provides an opportunity to enhance fire detection. In order to integrate resources provided by multiple satellite platforms, the Hazard Mapping System (HMS), developed by the National Oceanic and Atmospheric Administration's (NOAA) National Environmental Satellite and Data Information Service (NESDIS), utilizes multiple geostationary and polar orbiting environmental satellites to

monitor fires across North America, Hawaii, and Puerto Rico. Fires are automatically detected using detection algorithms for each of the sensors, and quality control procedures applied by image analysts eliminate false fires and add hotspots that are not detected by the algorithms. Although the HMS was developed in 2001, efforts for comparison of the HMS data to accurate ground-based fire records have been limited [*Ruminski and Hanna*, 2008; 2010], because of the difficulty in collecting sufficient *in-situ* measurements, given the spatiotemporally dynamic nature of active fires [*Csiszar et al.*, 2006]. Previous work used Advanced Spaceborne Thermal Emission and Reflection Radiometer (ASTER) data to assess the performance of a subset of HMS fire pixels [*Schroeder et al.*, 2008b]. ASTER images from the Terra satellite provide a unique opportunity to assess active fires derived from MODIS due to their high-resolution, multi-spectral measurements within a ~60 km swath near the center of the MODIS swath. However, such analyses were limited to omission errors in ASTER fire detection [*Giglio et al.*, 2008] caused by the visual and spectral interpretation of ASTER data and cloud cover that may have masked the fire at time of satellite overpass. Consequently, ASTER data cannot fully replace ground-based fire data as a validation reference [*Morisette et al.*, 2005]. *Zhang et al.* [2011] evaluated the HMS fire detection rates using the 2005 National Fire Inventory (NFI) dataset which contains ~2900 fire events with ground-based measurements and is obtained from the 2005 Incident Status Summary (ICS-209) reports. Most of the fires recorded in the ICS-209 reports are large wildfires which occurred on federal lands. A large number of prescribed fires in the southeastern U.S. which are usually conducted on private lands are not included in the ICS-209 reports. From 2011, NFI started to include ground-based fire records collected by local air

quality and forest agencies in most states. Hence, the quality of NFI has been greatly improved since then because of the availability of these datasets. In addition, the 2005 NFI dataset is prone to errors in fire latitude, longitude, and extent of burned areas, and can only be used for general assessment of burned area estimated from satellite observations. Thus, more complete and accurate ground-based fire records are needed for further assessment of the HMS fire product.

Because wildfires are episodic events, determining fire times, locations, and emission rates is challenging and expensive. Consequently, the United States Environmental Protection Agency (USEPA) National Emissions Inventory (NEI) is often limited in information about the specific location and timing of major fire events. However, these data are essential for the Community Multiscale Air Quality (CMAQ) model to accurately predict concentrations of various air pollutants. One alternative is to retrieve these data on a near-real time basis from spaceborne sensors. Thus, the CMAQ simulations have become increasingly reliant on satellite-derived fire emissions for air quality forecasting [*Roy et al.*, 2007]. However, uncertainty in satellite-based fire locations and emissions can affect the accuracy of the pollutant emissions inventory prepared for the CMAQ model and cause errors in model estimated impact of fires on regional air quality [*Yang et al.*, 2011], which warrants an accuracy assessment of satellite-based fire detections for the CMAQ model.

USEPA is aware of the need of wildland fire emissions with detailed temporal and spatial information and has collaborated with U.S. Forest Service to develop 2011 national fire emission inventory (http://www.epa.gov/ttn/chief/net/2011nei/nei2011v2_tsd_14aug2015.pdf). It is also

the first time that they requested local burning records from both state and federal agencies and used these records together with satellite fire detection products to develop national wildland fire emission inventory. However, the satellite fire product has shown very different temporal and spatial characteristics compared with local burning records in the state of Georgia (http://www3.epa.gov/ttn/chief/firesummit/Tian.pdf). There is a concern of using satellite fire products to develop fire emission inventory to support policy making in air quality management practice.

The state of Georgia contains various land cover types in which wildfires are prone to occur, including forestland and swamp. In 2011, 8,650 wildfires burned ~461,588 acres in Georgia, according to 2011 NEI (ftp://ftp.epa.gov/EmisInventory/2011v6/v2platform). In addition, prescribed burning is widely used in the southeast for ecosystem management [*Hardy et al.*, 2001], particularly in Georgia with > 1 million acres burned annually [*Lee et al.*, 2005]. In 2011, 27,513 prescribed fires burned ~1,225,295 acres in Georgia. According to 2011 NEI, 50% of $PM_{2.5}$ emissions in Georgia are contributed by Wildland fires (http://www3.epa.gov/ttn/chief/firesummit/Tian.pdf). In addition, Biomass burning has been estimated to contribute 13% of $PM_{2.5}$ mass concentrations annually in the southeastern U.S. [*Zhang et al.*, 2010], representing an important emissions source of air pollution in this region. However, in Georgia, there are a large amount of small under-canopy fires, and the duration of these fires is usually a few hours. Only understory fuel is burned, while trees are unburned. The small and short-lived nature of those fires reduces the possibility for satellite sensors to detect them. Although the HMS can take advantage of both high spatial and temporal resolutions from

multiple satellite instruments and may have better chance to detect those fires, its ability has yet to be demonstrated. In addition, the SmartFire system [*Raffuse et al.*, 2012] has become a popular fire information system which incorporates both satellite and ground-based fire records from disparate sources for aggregating, associating, and reconciling wildland fire information. However, the appropriateness of using the satellite fire records directly in the system continues to be an important issue, especially in the southeastern U.S. Thus, it is essential to use all independent information available to assess the accuracy of fire detections derived from satellite sensors in this region.

The objective of this paper is to compare a subset of 2011 HMS fire pixels to a set of ground-based fire records from either observations or prescribed fire authorization data collected by various agencies in the state of Georgia. HMS fire detection rates by season, land use/land cover (LULC) type, and fire size were calculated, and a detection rate for each 12 x12 km^2 CMAQ grid cell was also determined thereby providing a clearer picture of fire detection properties for the HMS product. This work will also greatly improve understanding of uncertainties in fire emission inventory developed using satellite fire products.

2. Materials and Methods

2.1 HMS fire products

We obtained active fire detections during 2011 from the HMS website (http://satepsanone.nesdis.noaa.gov/FIRE/fire.html). Fire detections were obtained using multiple bands with the 4 micron bands as the primary bands from the geostationary imager on

GOES-13 (EAST) with a nominal spatial resolution of 4 km using the WildFire Automated Biomass Burning Algorithm (WF_ABBA), and the MODIS instruments onboard the National Aeronautics and Space Administration (NASA) Terra and Aqua satellites at a nominal spatial resolution of 1 km using the MOD14 (Terra) and MYD14 (Aqua) products, as well as AVHRR on NOAA-15/18/19/METOP-02 with a 1 km resolution using the Fire Identification, Mapping and Monitoring Algorithm (FIMMA) [*He and Li*, 2012]. While the nominal spatial resolution for each of the sensors is provided, there can be considerable degradation for ground locations at increasing distance from nadir. Since GOES-13 maintains a constant orbit relative to the earth's surface, the pixel resolution is also constant for any given ground location. Over Georgia, this is approximately 5 km. For the polar orbiting MODIS and AVHRR sensors, the orbit changes daily such that the resolution at any given ground location will vary and can be as great as 5 km near the edge of the swath. GOES-13 provides imagery at a 15 minute frequency, while MODIS and AVHRR provide twice daily coverage per spacecraft. Since the HMS was utilizing 6 different polar spacecraft at this time, each in a different temporal and spatial orbit, this nearly assured that locations in Georgia would receive nominal 1 km resolution at least once per day and thus receive the benefit of high temporal frequency from GOES and high spatial resolution from polar sensors. In addition to the automated detections, many fire locations are added to the dataset manually by the satellite analyst for suspected fires that the automated algorithms have not detected. The dataset includes the latitude and longitude of each fire detection, the date on which the fire was detected, and the sensor that detected the fire. In 2011, the HMS shows the majority

of fire detections in the spring (230,440), and the fewest in the winter (82,195). It should be noted that multiple HMS fire detections may detect the same fire incident.

2.2 Ground-based fire records

We compiled a dataset of fire records, containing prescribed fire authorizations issued by the Georgia Forestry Commission (GFC), wildfires observed and recorded by the GFC and military bases, and prescribed fires and wildfires recorded by the Fish and Wildlife Service and U.S. Forest Service as part of their internal fire monitoring systems. Each record included the longitude, latitude, and burned area of the fire incident, and the date on which the fire occurred. There is only one single burned area value for each fire record, and no daily incremental information is included. The minimum size of fires recorded is 0.01 acres, which applies to all fires of any cause. In the case of burn authorizations, fires were assumed to have covered the requested burn acreage, although this assumption was not unequivocally confirmed with follow-up data. Given that authorizations are requested and issued the morning of the prescribed burn when detailed weather forecasts are available, it is rare for authorized burns not to occur. Also, GFC dispatchers ask whether or not burns are continuations of previously authorized burns to avoid double recording of prescribed burns for the same property parcel. Although the coordinates of each fire were provided, many of them may be approximations of real fire locations, especially when the coordinates were not directly provided but estimated from the centroids of zip codes, city, or county. As a result, the ground-based fire data included a variable "MatchType" to reflect the accuracy of the latitudes and longitudes, including "provided lat/lon",

"geocoding", "zip code", "city", and "county". In this study, the Match Types of "city", and "county" were discarded because the accuracy of these fire coordinates are considered insufficient. Figure 1 illustrates the distributions of fire counts and burned areas by match type. It shows that 78% of total fire observations fell into match types "provided lat/lon", "geocoding", and "zip code", and were subsequently included in this analysis. An accurate lat/lon is provided for 99% of wildfires, while 44% of prescribed burns are provided with coordinates at zip code levels. Figure 2 illustrates the seasonal distributions of fire counts and burned areas and shows that more fires occurred in winter and spring than in summer and fall. The differences are mainly caused by prescribed burns, the majority of which occurred in winter and spring, while wildfires are more evenly distributed among seasons. In addition, for different seasons, 76 to 94% of fire counts and 59 to 98% of burned areas were considered for inclusion in this analysis as they fall into match types "provided lat/lon", "geocoding", and "zip code". Figure 3 depicts the distributions of fire counts and burned areas by LULC type as determined from 2011 National Land Cover Database (NLCD). The number of fire incidents is the greatest (34% of total fire incidents) in forest areas and the least (0.2% of total fire incidents) in barren land, which is also true if prescribed burns and wildfires are counted separately. A large number of fires also occurred in developed areas (25% of total fire incidents). Considering that only 60% of fire counts and 44% of burned acreage in developed areas are qualified for this study (i.e., falling into the first three match types with highly accurate latitudes and longitudes), many of those fire observations may be falsely categorized to developed areas because of their less accurate coordinates and classification errors from 2011 NLCD. For example, the NLCD level II overall

accuracy are 79% and 78% for 2001 and 2006 land cover, respectively [*Wickham et al.*, 2013]. Likewise, a small number of fire observations are categorized to water regions, and they may be falsely classified due to the similar reasons.

Although fire behavior was not observed or recorded for the studied fires, knowledge of the LULC categories where fires occurred suggests that fires were surface fires (<5 m flame lengths) fueled by dead and live herbaceous vegetation, leaf litter (including pine needles), fine dead wood, and duff/organic soil where it exists, given that crown fires involving trees generally do not occur in the region. Possible exceptions are in shrub lands, and wetlands dominated by shrubs, where the crowns of shrubs can burn with flame lengths up to 10 m.

[Insert Figure 1-3 about Here]

2.3 Methods

To calculate the detection rates, a spatiotemporal match needs to be employed between ground-based fire records and HMS fire detections (Figure 4). A fire spot map was first generated for ground records and HMS fire detections, respectively using their coordinates. Each ground record was then linked to a corresponding 12 x 12 km^2 CMAQ grid cell which it falls inside by spatial join using ArcGIS [*ESRI*, 2011], in order to view the geographic distribution of fire detections among CMAQ grid cells. For ground records, a circular buffer centered at each fire spot with its area equal to its reported burned area was created. However, because the spatial coverage of the actual fire can be irregular and could far exceed the coverage of the circular buffer, *Zhang et al.* [2011] increased the radius of the buffer zone to up to ten times to avoid

omitting genuine matches between burn scar coverage and active fire detections. They determined the final fire counts when the rate of increasing counts reached the first minimum with increasing buffer zone. In this study, we conducted a similar sensitivity analysis (Figure 5) and determined the buffer radius once the rate of increasing fire detections reached the first minimum with increasing buffer radius. Thus we adopted the ten times radius to generate the circular buffer centered at each ground-based fire point to reduce the possibility of omission in the process of data match. This method helped minimize navigation inaccuracies in the satellite data which could cause an offset of 5 km or more from the true fire location. Geo-location errors vary by sensors with MODIS likely having the smallest. For HMS fire detections, a 4 x 4 km^2 square buffer was generated for each GOES fire pixel, while a 1 x 1 km^2 square buffer was created for each MODIS and AVHRR fire pixel based on the nominal spatial resolution of each satellite product. It is noted that the actual pixel resolution for the AVHRR and MODIS sensors can be much larger (4 to 5 km) near the edge of the scan, and the resolution of GOES could be as large as 5 km over Georgia. Thus, data match may be negatively impacted in these areas. The spatiotemporal match between circular buffers of ground-based fire records and HMS fire pixels was then conducted using ArcGIS [*ESRI*, 2011]. If a circular buffer centered at a ground-based fire point was spatially overlaid with a HMS fire pixel, and the date on which the fire occurred was equal to the date on which the HMS fire was detected, that fire was considered successfully detected by the HMS fire product. The detection rate was calculated using the following equation

$$Detection\ Rate = \frac{the\ Number\ of\ Fire\ Records\ Detected\ by\ HMS}{the\ Number\ of\ Total\ Fire\ Records} \times 100\% \quad (1)$$

The detection rates by season, LULC type, and fire size were calculated to investigate the impacts of seasons, LULC types, and fire sizes on the ability of the HMS fire product to detect fires. We also calculated the detection rate for each CMAQ grid cell to examine the spatial pattern of HMS fire detection rates in the state of Georgia.

[Insert Figure 4-5 about Here]

3. Results

3.1 HMS fire detection rates by season, LULC type, and fire size

Figure 6a illustrates the HMS fire detection rates by season. The result shows that more fires occur in winter and spring than in summer and fall. The detection rates are also higher in winter and spring (12 and 13%, respectively) than in summer and fall (3 and 6%, respectively). However, fire counts in winter are higher than those in spring, while the detection rates in winter are lower than that in spring. This is also true for the results between summer and fall, which indicates that the fluctuation of fire counts do not correspond well with that of detection rates for the four seasons, and high fire counts do not necessarily lead to high detection rates.

In contrast, the fluctuation of the percentages of large fires has a good agreement with that of detection rates. For example, the percentages of large fires (> 0.19 km^2, the mean fire size in the study region) that occurred in winter and spring (20.1 and 26.8%, respectively) are higher than those that occurred in summer and fall (5.5 and 5.6%, respectively). This suggests that the HMS has a greater ability to detect fires in seasons during which large fires occur more frequently.

Figure 6b depicts the HMS fire detection rates by LULC types. The results are consistent with previous studies. For instance, *Li et al.* [2003] found that fire omission errors are low over

forested regions, while moderate errors were found over semi-arid areas, as well as along rivers and around lakes. *Pu et al.* [2007] also reported low fire omission errors over forested areas. It also shows that the distribution of detection rates does not correspond well with that of fire counts, and the relatively high detection rates (>10%) are obtained in forest land, planted/cultivated land, shrub land, and wetlands, which are land covers prone to large fires. The mean percentage of large fires (> 0.19 km^2) that occurred in these land cover types (22.1%) is higher than those that occurred in others (14.3%). This again suggests that, not surprisingly, fire size has a significant impact on the fire detection rate. Other causes of low detection rates may be attributed to the contamination of solar reflection for barren land and fuel types/patterns used in prescribed fires for cropland/agricultural land [*He and Li*, 2011].

Figure 6c illustrates the HMS fire detection rates by fire size. These results distinctly show that the detection rates increase steadily from 3% to 80% with the increase of the fire size. In addition, these results also indicate that most of the fires that occurred in the study region are small fires (< 0.19 km^2), which account for 80% of all fires. Consequently, too many small fires lead to the relatively low detection rate by the HMS for all fire incidents in the entire study region, which is 12%. However, the burned area of all the fires detected by the HMS represents 57% of the total area burned.

To assess the performance of each single automated algorithm, the detection rates for fire detections directly derived from MODIS, ABBA, and FIMMA were also calculated and plotted in Figure 6c, respectively. These results indicate that MODIS reached relatively higher detection rates than FIMMA and ABBA. Both MODIS and FIMMA outperform ABBA for small fires,

while ABBA has high detection rates for large fires. The overall fire detection rates of the HMS increase substantially by incorporating all three sets of satellite sensors.

[Insert Figure 6 about Here]

3.2 HMS fire detection rates for the CMAQ grid

Figure 7a illustrates the seasonal and annual HMS fire detection rates for each CMAQ grid cell to reveal the spatial patterns of detection rates within Georgia. Although fire incidents mostly occurred in southern Georgia, the detection rates show different spatial patterns from those of fire counts in both seasonal and annual maps. Grid cells with high detection rates do not cluster in southern Georgia. Instead, they are spread all over the entire state, and no systematic pattern can be found. By comparing the map of ground-based fire records with their corresponding burned areas simulated using circular buffers (Figure 7b), it was found that clusters of grid cells with high detection rates match well with clusters of large fires (in red circle), indicating that grid cells with high fire detection rates are generally located in areas where large fires occurred frequently. A regression analysis confirms a statistically significant ($p < 0.0001$) and positive relationship between detection rates and mean fire sizes for CMAQ grid cells, suggesting that fire size has a significant impact on detection rate. These results also show that there are more grid cells with high detection rates in winter and spring than in summer and fall, which closely follows the results from our seasonal detection rate analysis and corroborates that overall detection rates are generally higher in winter and spring than in summer and fall. The annual map shows fewer grid cells with high detection rates than the winter and spring maps. This is

perhaps due to numerous grid cells with low detection rates in summer and fall which reduces the detection rates within those grid cells for the entire year.

[Insert Figure 7 about Here]

4. Discussion

Our assessment of detection rates of the HMS are consistent with multiple previous studies which report increased fire detection rates (decreased omission errors) with increased fire sizes [*Boles and Verbyla*, 2000; *Hantson et al.*, 2013; *Ruminski and Hanna*, 2010; *Schroeder et al.*, 2008a]. Our results also show that fire detection rates of the HMS increase steadily with the increase of fire sizes, and fire sizes have a statistically significant and positive impact on detection rates. This pattern is attributable to larger fires having higher rates of energy release. Also, they typically burn longer and thus are more likely to be detected by mid-wave infrared channels of satellite sensors. Although it is possible that the pattern is confounded by the effects of season and LULC type, it is most likely that the variation among season and LULC categories simply reflects the size of burns associated with those times and cover types.

MODIS algorithm has a relatively better performance than FIMMA and ABBA likely because MODIS is a more suitable sensor for fire detection than GOES imager or AVHRR due to better pixel-level spatial radiometric sensitivity and appropriate dynamic range. For example, MODIS has high gain band (band 22, 3.96 um saturating at ~354 K, with less solar contribution) comparing to AVHRR 3.7 um band (saturating at ~336 K, more solar contribution). MODIS also has the low gain band 21 (3.96 um saturating at ~500 K) which is used by MODIS algorithm

when band 22 is not available or has saturated, particularly in summer time when there is strong solar reflection. In addition, MODIS data probably has the smallest geo-location error. Another reason could be that the MODIS algorithm is more robust than FIMMA. FIMMA has had no changes since around 2002 and 2003, while MODIS algorithm has had improvements. Both MODIS algorithm and FIMMA outperform ABBA for small fires due to the higher spatial resolution of MODIS and AVHRR, while ABBA has a good performance for large fires. Although the coarser nominal resolution of the GOES imager limits the performance of the WF_ABBA product for small fires [*Schroeder et al.*, 2008b], unlike MODIS and AVHRR, the high sampling frequency of GOES observations could capture fires of a limited duration or during a short cloud-free period [*Zhang et al.*, 2011]. By integrating multiple satellite-derived fire detection products, the HMS takes advantage of high temporal (e.g., GOES) and spatial (e.g., MODIS and AVHRR) resolutions at the same time and reduce the possibility of missing small and short-lived fires, as well as fires obstructed by cloud cover [*Zhang et al.*, 2011].

Our analysis includes a few limitations. First, there is uncertainty in the location information of fires in the ground-based fire records. Unarguably, the accuracy of fire locations has a significant impact on the fire detection rates. The ground data provide five match types to evaluate the accuracy of the coordinates. In this study, the match types “provided lat/lon”, “geocoding”, and “zip code” were considered high quality and included, while types “city” and “county” were discarded because a city or county is so large that the provided coordinates may be too far away from the real location of the fire event. Although a zip code also could be too large in size for some small fires, leading to mislocation of those fires, we still adopted type “zip code” in this

study, because a large number of recorded fires belong to this type, and we want to include as many ground records as possible. In addition, the mislocation caused by the type "zip code" should be small compared to types "city" and "county", and our buffering approach should accommodate for this error.

Second, although there is a burned area associated with each ground-based fire record, the actual shape of the burn scar is unknown. One of the solutions is using circular buffers with their sizes equal to the corresponding burned area to simulate the shapes of burn scars. This inevitably causes large omission errors since the spatial coverage of the actual burn scar may cover large areas outside the circular buffer. There are also inaccuracies in the satellite data locations due to inherent errors in the navigation of the imagery and subsequent offsets introduced when the imagery is reprojected. For example, GOES pixels have a 4 km resolution at nadir (approximately 5 km over Georgia). A one pixel offset in navigation could result in an 8 km distance between the actual fire and the GOES location if the fire was near a corner of the GOES pixel and the GOES location is the center of the pixel. The use of the enlarged buffers helps to address this situation. Our sensitivity analysis demonstrates that matches between HMS fire pixels and ground-based fire points increase with increasing buffer zone. However, to accurately determine how large buffer zones should be remains a challenge. Too small or too large buffer zones inevitably lead to under-matches or over-matches. In this study, we adopted a similar method proposed by *Zhang et al.* [2011] determining the buffer radius once the rate of increasing fire detections reached the first minimum with increasing buffer zone, which is ten times the burn-area equivalent radius in this study, to build the circular buffer. This method significantly

reduces the omission errors and increases the detection rates. It should be noted that this method is suitable for our study area, since most fires in this region are small fires, and may not be appropriate for applications in the western U.S. where very large fires occur.

Third, our method of data matching requires that both recorded fires and detection by satellite sensors occur on the same date. This may also lead to omission errors because both MODIS and AVHRR instruments only scan a location twice a day, and their views may be blocked by cloud cover, although the utilization of six spacecraft affords potentially 12 looks per day over the region. While GOES has a much higher temporal resolution (nominally every 15 minutes), its low spatial resolution may reduce fire detection rates [*Schroeder et al.*, 2008b]. However, in this study, we did not find this to cause a large number of omissions in our spatiotemporal match between ground records and HMS fire detections. Hence, we focused on reported and detected fires on the same date.

Finally, we did not examine the commission errors (false detections) of the HMS fire product, because only parts of the ground-based fire records (types 0, 1, and 2) have relatively accurate coordinates and are included in this analysis. Additionally, it is possible that there could be actual fires that are not included in the ground report datasets. It could be a future direction when more complete ground data with higher quality are available.

5. Conclusions

This paper compares the 2011 HMS fire product to a set of ground-based fire records, including observations and burn authorizations, in the state of Georgia. It extends previous efforts to evaluate satellite fire detections by focusing mostly on small and frequent fires. The results show

that MODIS algorithm and FIMMA outperform ABBA for small fires due to the higher nominal spatial resolution of MODIS and AVHRR, and ABBA has a good performance for large fires due to the higher sampling frequency of GOES imagers. The detection rates of the hybrid HMS increase substantially by incorporating multiple satellite sensors. The results also show that the detection rate of the HMS fire product increases dramatically from 3% to 80% with an increase in fire size from less than 0.02 km^2 to larger than 2 km^2, resulting in detection of approximately 12% of all recorded fires which represent approximately 57% of the total area burned. Additionally, we find that spatial patterns of detection rates are not in accordance with those of fire counts for both seasonal and annual maps, and no systematic patterns can be found. Instead, the CMAQ grid cells with high detection rates are generally located in areas where large fires occurred frequently, and a statistically significant and positive relationship was found between detection rates and mean fire sizes for CMAQ grid cells. These results suggest that fire size has a significant impact on the detection rate. Seasonal analysis shows that the detection rates in winter and spring are higher than those in summer and fall, because the percentages of large fires (> 0.19 km^2) that occurred in winter and spring are higher than those that occurred in summer and fall. The LULC analysis shows that detection rates are higher in LULC types that are prone to large fires.

Acknowledgements:

This publication was made possible by USEPA grant R834799. Its contents are solely the responsibility of the grantee and do not necessarily represent the official views of the USEPA.

Further, USEPA does not endorse the purchase of any commercial products or services mentioned in the publication. This work was also supported by NASA Applied Sciences Program (grant No. NNX11AI53G, PI: Liu) and NIH grant R01ES019897. The HMS data used in this paper are available free through the links provided in the Materials and Methods section of the paper. Inquiries regarding the ground fire observation data should be directed to Dr. Di Tian (Di.Tian@dnr.ga.gov) at the Georgia Department of Natural Resources.

References

Boles, S. H., and D. L. Verbyla (2000), Comparison of Three AVHRR-Based Fire Detection Algorithms for Interior Alaska, *Remote Sens. Environ.*, *72*(1), 1-16, doi:http://dx.doi.org/10.1016/S0034-4257(99)00079-6.

Certini, G. (2005), Effects of fire on properties of forest soils: a review, *Oecologia*, *143*(1), 1-10, doi:10.1007/s00442-004-1788-8.

Csiszar, I., J. T. Morisette, and L. Giglio (2006), Validation of active fire detection from moderate-resolution satellite sensors: The MODIS example in northern Eurasia, *IEEE Trans. Geosci. Remote Sensing*, *44*(7), 1757-1764, doi:10.1109/tgrs.2006.875941.

Csiszar, I., W. Schroeder, L. Giglio, E. Ellicott, K. P. Vadrevu, C. O. Justice, and B. Wind (2014), Active fires from the Suomi NPP Visible Infrared Imaging Radiometer Suite: Product status and first evaluation results, *Journal of Geophysical Research: Atmospheres*, *119*(2), 2013JD020453, doi:10.1002/2013jd020453.

ESRI (2011), ArcGIS desktop: release 10, *Environmental Systems Research Institute, Redlands, California, USA*.

Fearnside, P. (2000), Global Warming and Tropical Land-Use Change: Greenhouse Gas Emissions from Biomass Burning, Decomposition and Soils in Forest Conversion, Shifting Cultivation and Secondary Vegetation, *Clim. Change*, *46*(1-2), 115-158, doi:10.1023/a:1005569915357.

Giglio, L., I. Csiszar, Á. Restás, J. T. Morisette, W. Schroeder, D. Morton, and C. O. Justice (2008), Active fire detection and characterization with the advanced spaceborne thermal

emission and reflection radiometer (ASTER), *Remote Sens. Environ.*, *112*(6), 3055-3063, doi:http://dx.doi.org/10.1016/j.rse.2008.03.003.

Giglio, L., J. Descloitres, C. O. Justice, and Y. J. Kaufman (2003), An Enhanced Contextual Fire Detection Algorithm for MODIS, *Remote Sens. Environ.*, *87*(2–3), 273-282, doi:http://dx.doi.org/10.1016/S0034-4257(03)00184-6.

Hantson, S., M. Padilla, D. Corti, and E. Chuvieco (2013), Strengths and weaknesses of MODIS hotspots to characterize global fire occurrence, *Remote Sens. Environ.*, *131*(0), 152-159, doi:http://dx.doi.org/10.1016/j.rse.2012.12.004.

Hardy, C. C., S. M. Hermann, and R. E. Mutch (2001), The Wildland Fire Imperative, in *Smoke management guide for prescribed and wildland fire: 2001 edition*, edited by C. C. Hardy, R. D. Ottmar, J. L. Peterson, J. E. Core and P. Seamon, National Interagency Fire Center, Boise, ID.

He, L. M., and Z. Q. Li (2011), Enhancement of a fire-detection algorithm by eliminating solar contamination effects and atmospheric path radiance: application to MODIS data, *Int. J. Remote Sens.*, *32*(21), 6273-6293, doi:10.1080/01431161.2010.508057.

He, L. M., and Z. Q. Li (2012), Enhancement of a fire detection algorithm by eliminating solar reflection in the mid-IR band: application to AVHRR data, *Int. J. Remote Sens.*, *33*(22), 7047-7059, doi:10.1080/2150704x.2012.699202.

Justice, C. O., L. Giglio, S. Korontzi, J. Owens, J. T. Morisette, D. Roy, J. Descloitres, S. Alleaume, F. Petitcolin, and Y. Kaufman (2002), The MODIS fire products, *Remote Sens. Environ.*, *83*(1–2), 244-262, doi:http://dx.doi.org/10.1016/S0034-4257(02)00076-7.

Lee, S., K. Baumann, J. J. Schauer, R. J. Sheesley, L. P. Naeher, S. Meinardi, D. R. Blake, E. S. Edgerton, A. G. Russell, and M. Clements (2005), Gaseous and particulate emissions from prescribed burning in Georgia, *Environ. Sci. Technol.*, *39*(23), 9049-9056, doi:10.1021/es0515831.

Li, Z. Q., R. Fraser, J. Jin, A. A. Abuelgasim, I. Csiszar, P. Gong, R. Pu, and W. Hao (2003), Evaluation of algorithms for fire detection and mapping across North America from satellite, *J. Geophys. Res.-Atmos.*, *108*(D2), doi:10.1029/2001jd001377.

Lin, J. C., T. Matsui, R. A. Pielke, and C. Kummerow (2006), Effects of biomass-burning-derived aerosols on precipitation and clouds in the Amazon Basin: a satellite-based empirical study, *Journal of Geophysical Research: Atmospheres*, *111*(D19), D19204, doi:10.1029/2005jd006884.

Morisette, J. T., L. Giglio, I. Csiszar, and C. O. Justice (2005), Validation of the MODIS active fire product over Southern Africa with ASTER data, *Int. J. Remote Sens.*, *26*(19), 4239-4264, doi:10.1080/01431160500113526.

Oliva, P., and W. Schroeder (2015), Assessment of VIIRS 375 m active fire detection product for direct burned area mapping, *Remote Sens. Environ.*, *160*(0), 144-155, doi:http://dx.doi.org/10.1016/j.rse.2015.01.010.

Prins, E. M., and W. P. Menzel (1992), Geostationary satellite detection of bio mass burning in South America, *Int. J. Remote Sens.*, *13*(15), 2783-2799, doi:10.1080/01431169208904081.

Prins, E. M., and W. P. Menzel (1994), Trends in South American biomass burning detected with the GOES visible infrared spin scan radiometer atmospheric sounder from 1983 to 1991, *Journal of Geophysical Research: Atmospheres*, *99*(D8), 16719-16735, doi:10.1029/94jd01208.

Pu, R. L., Z. Q. Li, P. Gong, I. Csiszar, R. Fraser, W. M. Hao, S. Kondragunta, and F. Z. Weng (2007), Development and analysis of a 12-year daily 1-km forest fire dataset across North America from NOAA/AVHRR data, *Remote Sens. Environ.*, *108*(2), 198-208, doi:10.1016/j.rse.2006.02.027.

Raffuse, S. M., N. K. Larkin, P. W. Lahm, and Y. Du (2012), Development of Version 2 of the Wildland Fire Portion of the National Emissions Inventory, paper presented at 20th International Emission Inventory Conference, Tampa, Florida, August 13 - 16, 2012.

Roy, B., G. A. Pouliot, A. Gilliland, T. Pierce, S. Howard, P. V. Bhave, and W. Benjey (2007), Refining fire emissions for air quality modeling with remotely sensed fire counts: A wildfire case study, *Atmospheric Environment*, *41*(3), 655-665, doi:http://dx.doi.org/10.1016/j.atmosenv.2006.08.037.

Ruminski, M., and J. Hanna (2008), Validation of Remotely Sensed Fire Detections Using Ground and Aircraft Reports, *American Geophysical Union Fall Meeting 2008*, San Francisco, California.

Ruminski, M., and J. Hanna (2010), A Validation of Automated and Quality Controlled Satellite Based Fire Detection, *American Geophysical Union Fall Meeting 2010*, San Francisco, California.

Sapkota, A., J. M. Symons, J. Kleissl, L. Wang, M. B. Parlange, J. Ondov, P. N. Breysse, G. B. Diette, P. A. Eggleston, and T. J. Buckley (2005), Impact of the 2002 Canadian forest fires on particulate matter air quality in Baltimore City, *Environ. Sci. Technol.*, *39*(1), 24-32, doi:10.1021/es035311z.

Schroeder, W., E. Prins, L. Giglio, I. Csiszar, C. Schmidt, J. Morisette, and D. Morton (2008a), Validation of GOES and MODIS active fire detection products using ASTER and ETM+ data, *Remote Sens. Environ.*, *112*(5), 2711-2726, doi:http://dx.doi.org/10.1016/j.rse.2008.01.005.

Schroeder, W., M. Ruminski, I. Csiszar, L. Giglio, E. Prins, C. Schmidt, and J. Morisette (2008b), Validation analyses of an operational fire monitoring product: The Hazard Mapping System, *Int. J. Remote Sens.*, *29*(20), 6059-6066, doi:10.1080/01431160802235845.

Slik, J. W. F., C. Bernard, M. Van Beek, F. Breman, and K. O. Eichhorn (2008), Tree diversity, composition, forest structure and aboveground biomass dynamics after single and repeated fire in a Bornean rain forest, *Oecologia*, *158*(3), 579-588, doi:10.1007/s00442-008-1163-2.

Stroppiana, D., S. Pinnock, and J. M. Gregoire (2000), The Global Fire Product: daily fire occurrence from April 1992 to December 1993 derived from NOAA AVHRR data, *Int. J. Remote Sens.*, *21*(6-7), 1279-1288, doi:10.1080/014311600210173.

Wickham, J. D., S. V. Stehman, L. Gass, J. Dewitz, J. A. Fry, and T. G. Wade (2013), Accuracy assessment of NLCD 2006 land cover and impervious surface, *Remote Sens. Environ.*, *130*, 294-304, doi:http://dx.doi.org/10.1016/j.rse.2012.12.001.

Yang, E. S., S. A. Christopher, S. Kondragunta, and X. Y. Zhang (2011), Use of hourly Geostationary Operational Environmental Satellite (GOES) fire emissions in a Community Multiscale Air Quality (CMAQ) model for improving surface particulate matter predictions, *J. Geophys. Res.-Atmos.*, *116*, doi:10.1029/2010jd014482.

Zhang, X., A. Hecobian, M. Zheng, N. H. Frank, and R. J. Weber (2010), Biomass burning impact on PM2.5 over the southeastern US during 2007: integrating chemically speciated FRM filter measurements, MODIS fire counts and PMF analysis, *Atmos. Chem. Phys.*, *10*(14), 6839-6853, doi:10.5194/acp-10-6839-2010.

Zhang, X., and S. Kondragunta (2008), Temporal and spatial variability in biomass burned areas across the USA derived from the GOES fire product, *Remote Sens. Environ.*, *112*(6), 2886-2897, doi:http://dx.doi.org/10.1016/j.rse.2008.02.006.

Zhang, X., S. Kondragunta, and B. Quayle (2011), Estimation of Biomass Burned Areas Using Multiple-Satellite-Observed Active Fires, *Geoscience and Remote Sensing, IEEE Transactions on*, *49*(11), 4469-4482, doi:10.1109/tgrs.2011.2149535.

Figure Captions

Figure 1. The distributions of ground-based fire counts (a) and burned area (b) by match type.

Figure 2. The distributions of ground-based fire counts (a) and burned area (b) by season.

Figure 3. The distributions of ground-based fire counts (a) and burned area (b) by LULC type.

Figure 4. The flow chart of the spatiotemporal match.

Figure 5. The sensitivity analysis for increasing buffer radius.

Figure 6. The HMS fire detection rates by season (a), LULC type (b), and fire size (c).

Figure 7. The seasonal and annual HMS fire detection rates for each CMAQ grid cell (a), and the spatial distribution of ground-based fire observations with their simulated burned area (b).

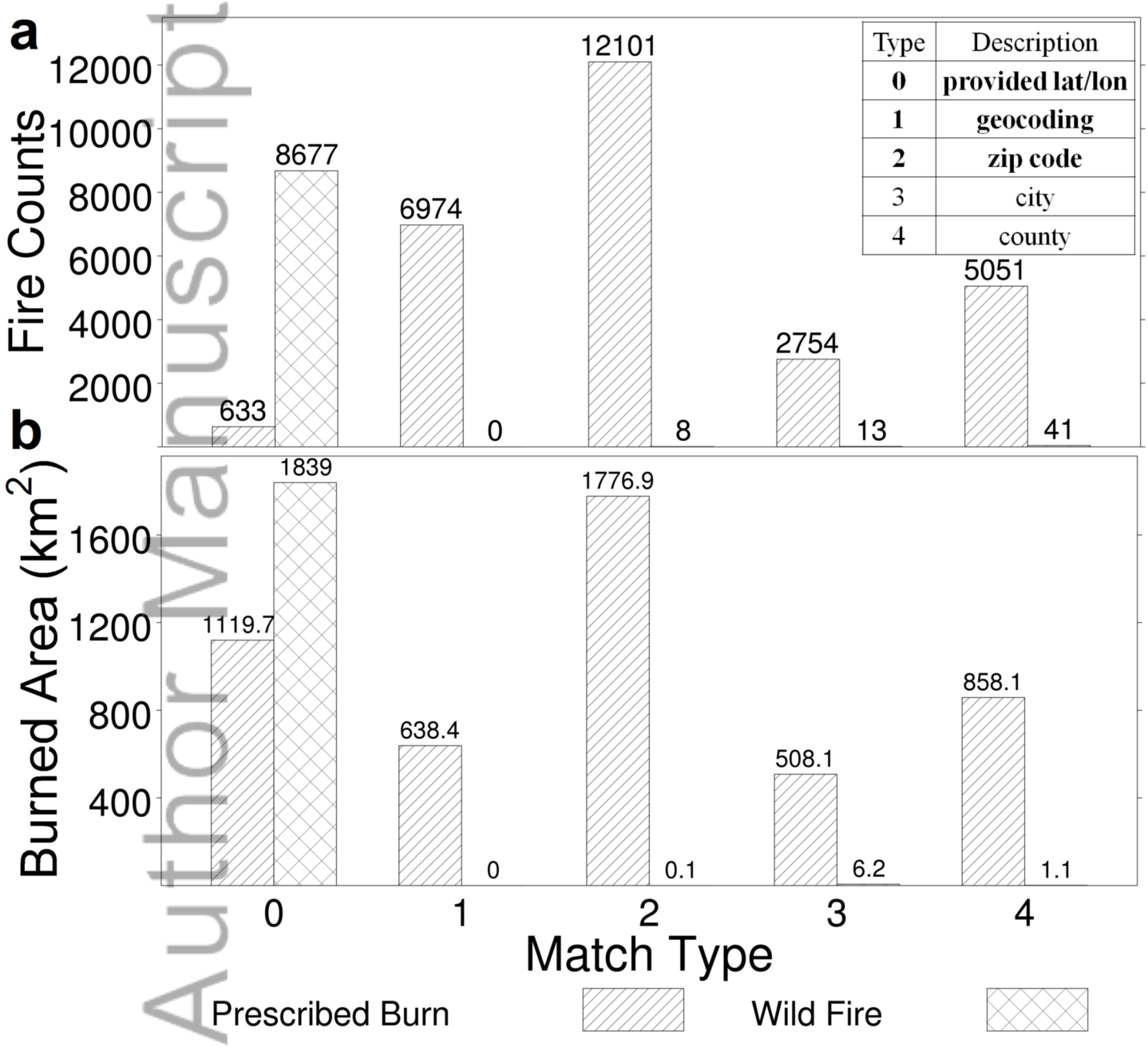

2015JD024448-f00-z-.tif

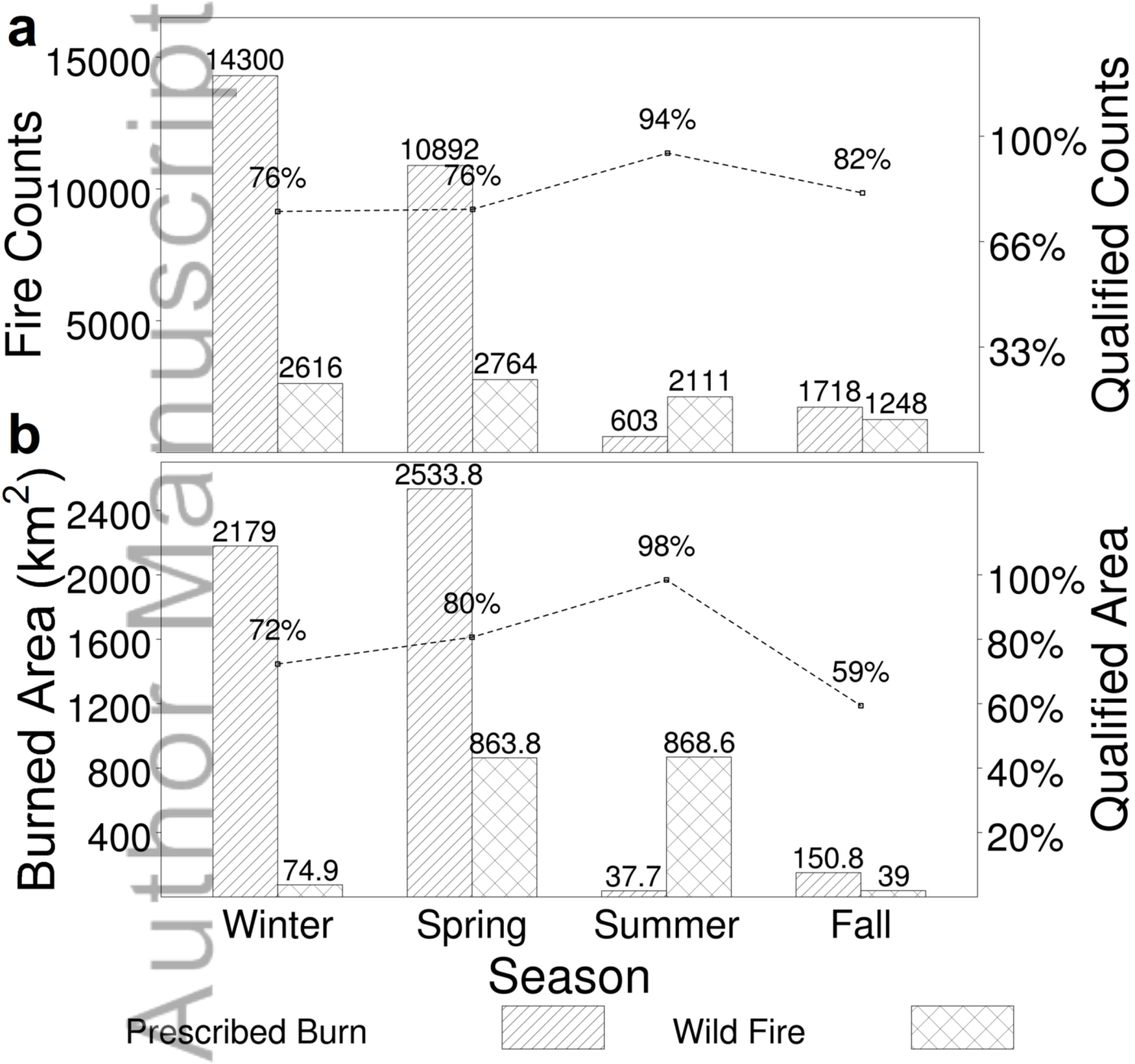

2015JD024448-f01-z-.tif

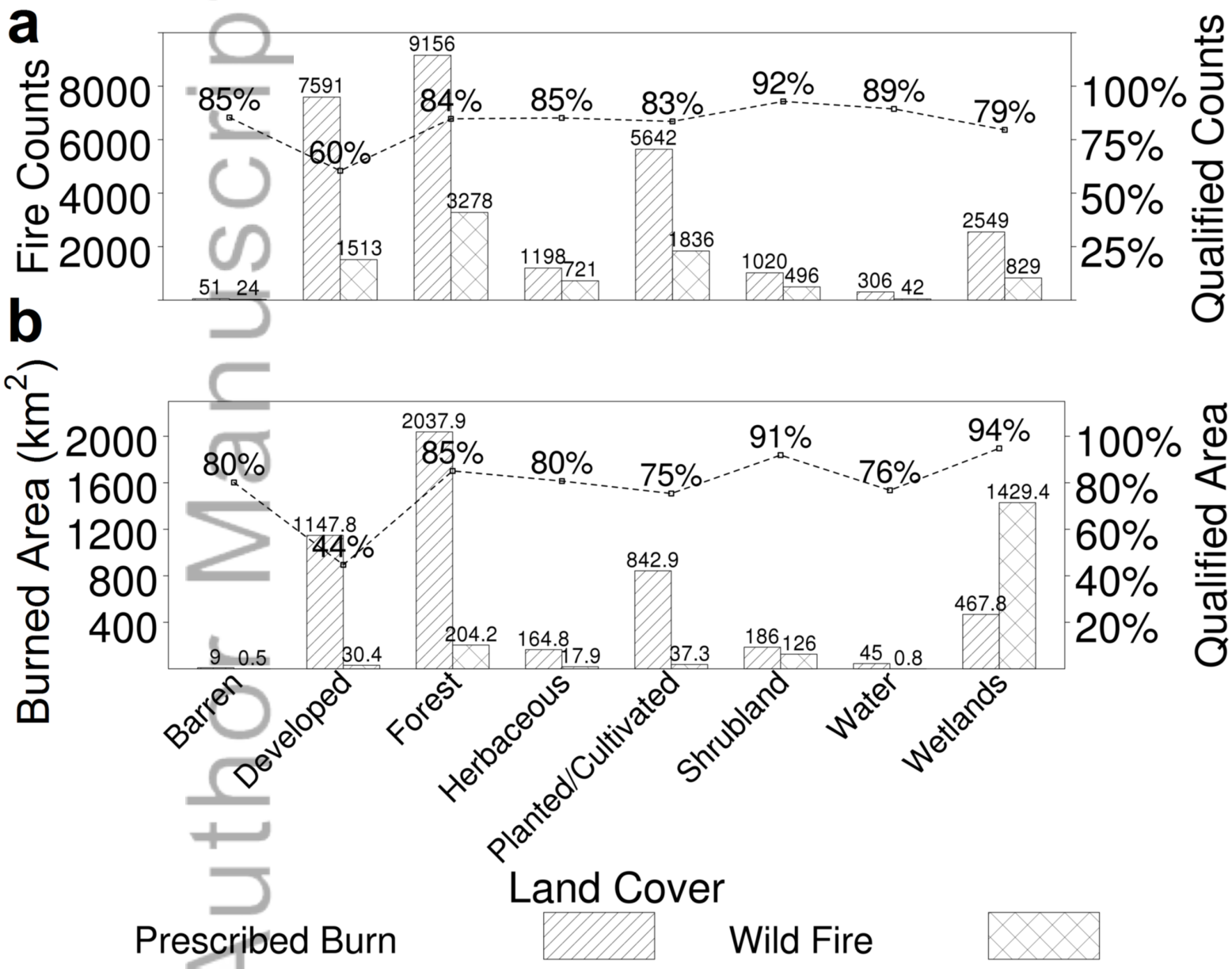

2015JD024448-f02-z-.tif

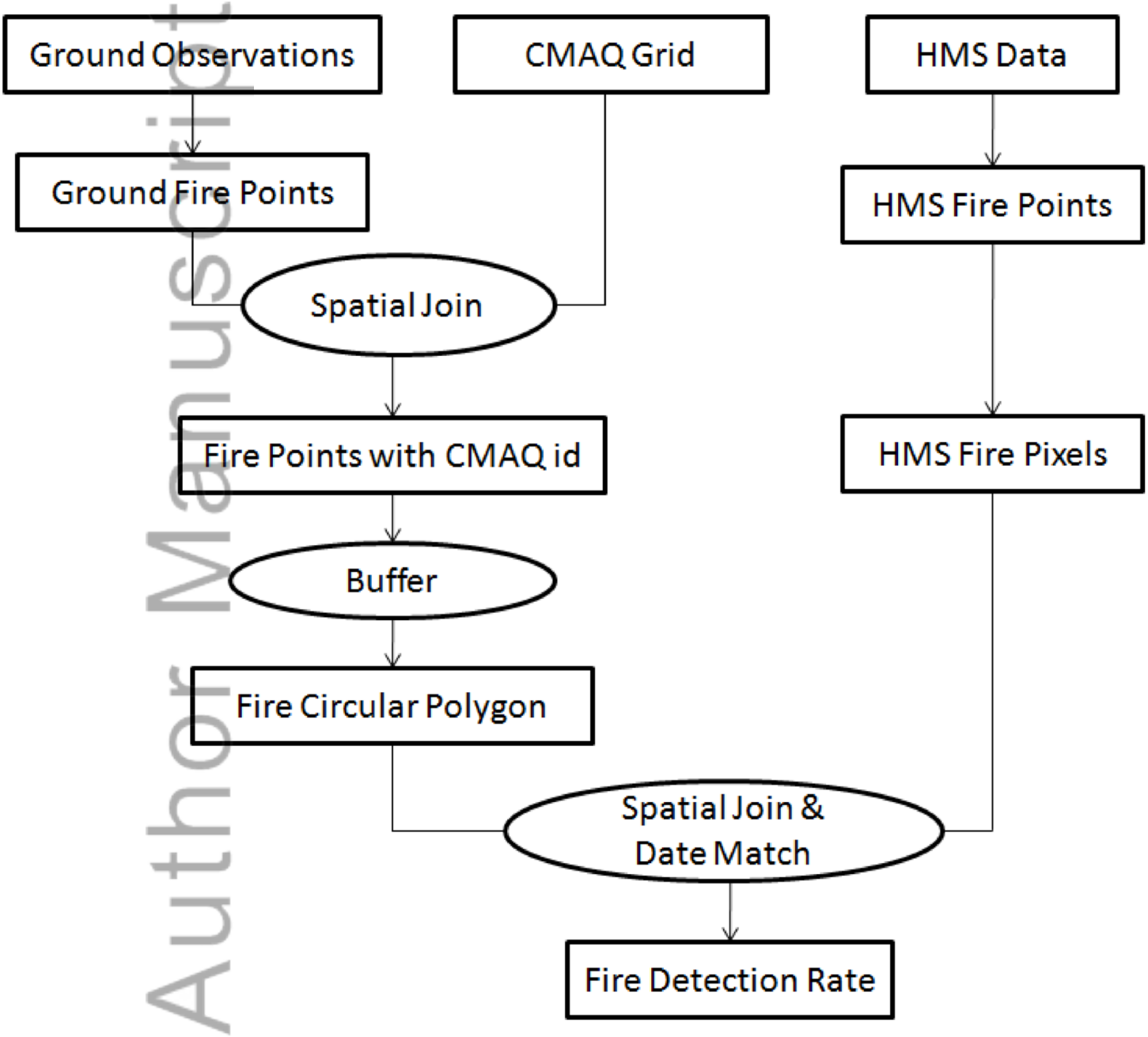

2015JD024448-f03-z-.tif

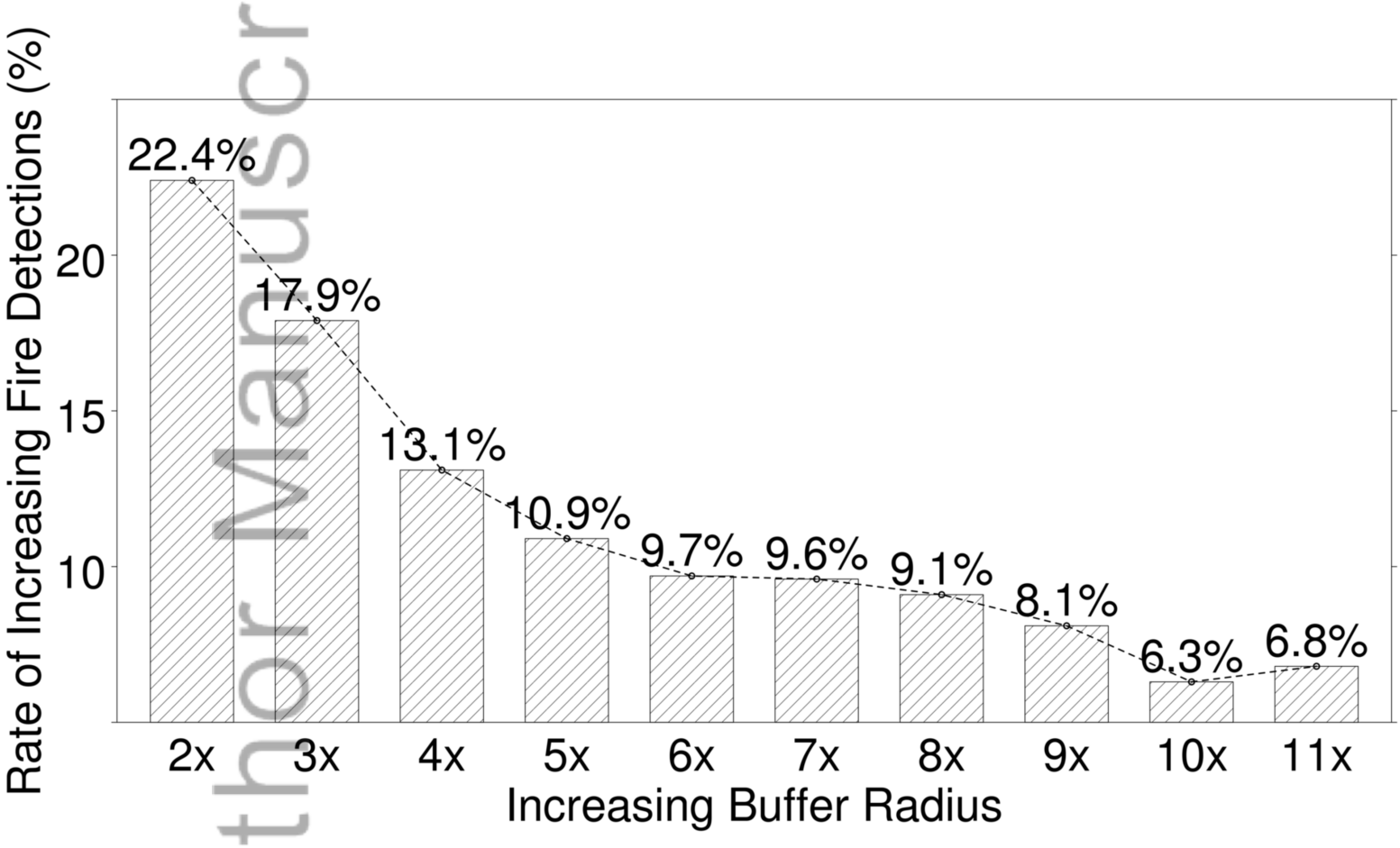

2015JD024448-f04-z-.tif

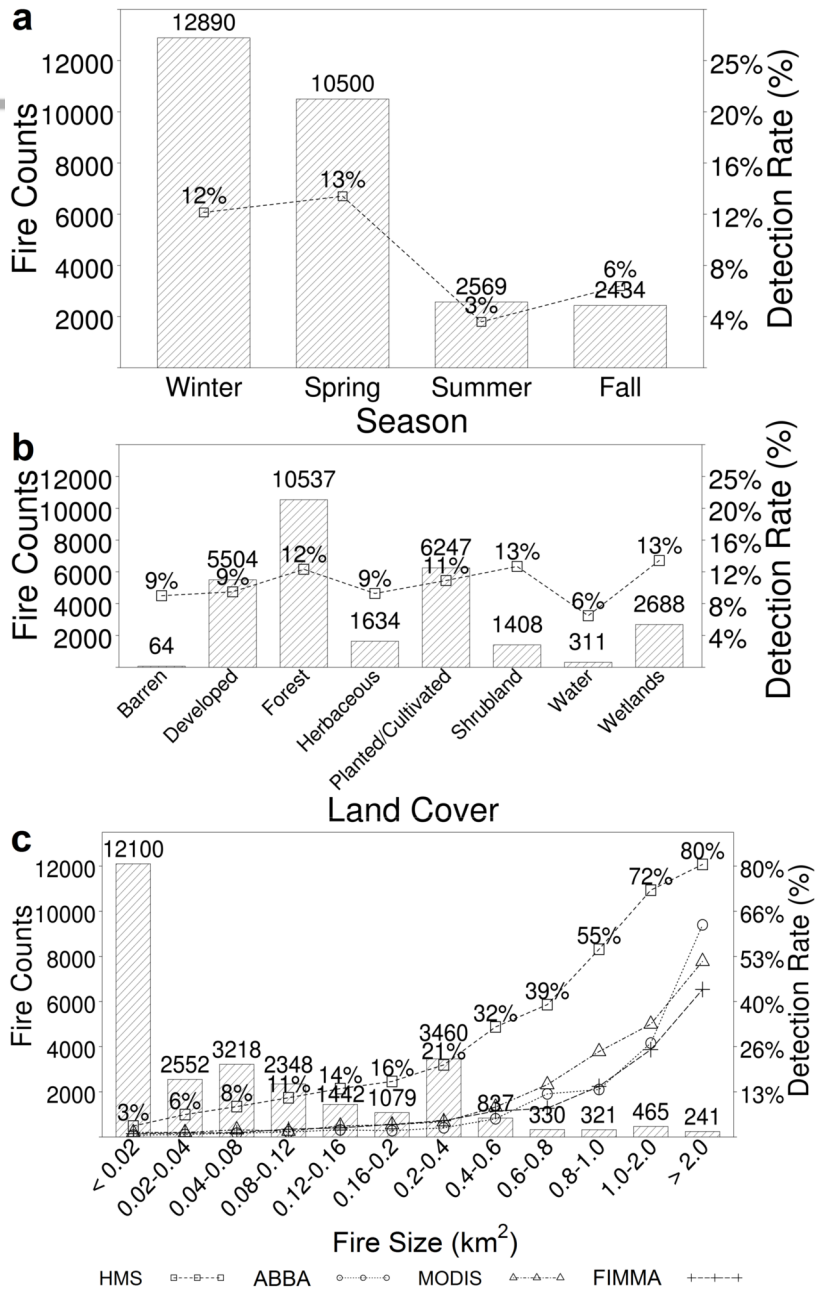

2015JD024448-f05-z-.tif

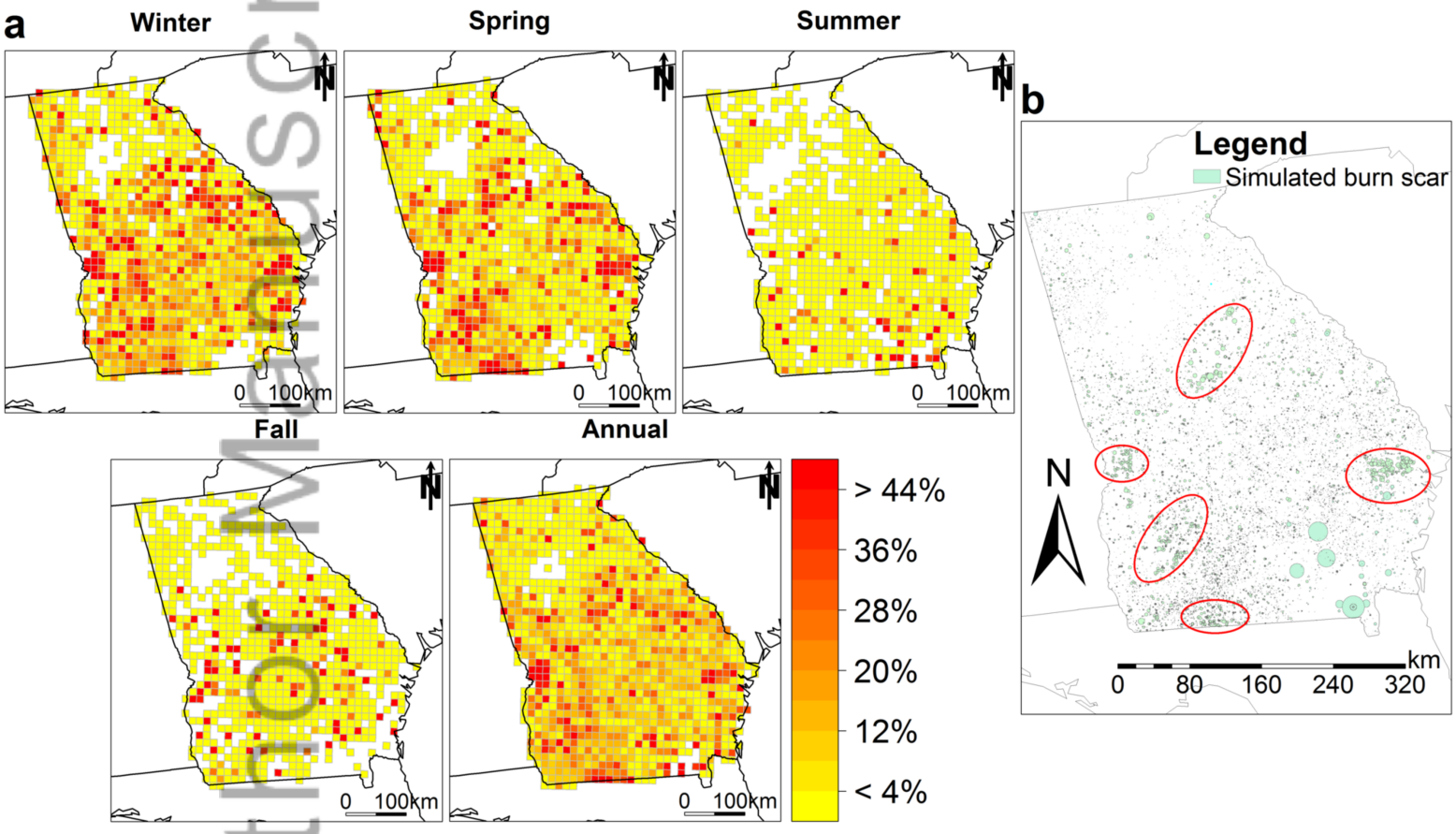

2015JD024448-f06-z-.tif